Bioactive Materials 4 (2019) 87–96

Contents lists available at ScienceDirect

Bioactive Materials

journal homepage: http://www.keaipublishing.com/biomat

Initial formation of corrosion products on pure zinc in saline solution

Yao Meng[a], Lijun Liu[a], Dawei Zhang[b], Chaofang Dong[b,c], Yu Yan[b], Alex A. Volinsky[d], Lu-Ning Wang[a,c,*]

[a] Beijing Advanced Innovation Center for Materials Genome Engineering, School of Materials Science and Engineering, University of Science and Technology Beijing, Beijing, 100083, China
[b] Institute for Advanced Materials and Technology, University of Science and Technology Beijing, Beijing, 100083, China
[c] State Key Laboratory for Advanced Metals and Materials, University of Science and Technology Beijing, Beijing, 100083, China
[d] Department of Mechanical Engineering, University of South Florida, Tampa, FL, 33620, USA

ARTICLE INFO

Keywords:
Zinc
Corrosion products
Saline
Degradation

ABSTRACT

Corrosion product formed on zinc sample during 2 weeks immersion in saline solution has been investigated. The corrosion layer morphology as well as its chemical composition, was analyzed using scanning electron microscopy (SEM), x-ray diffraction (XRD), x-ray photoelectron spectroscopy (XPS) and Fourier transform infrared spectroscopy (FTIR). Electrochemical measurement was used to analyze the corrosion behavior. Zinc oxide, zinc hydroxide and zinc hydroxide chloride were formed on zinc surface in saline solution. The thickness of corrosion layer increased with the time increased. The pure Zn has an estimated corrosion rate of 0.063 mm y^{-1} after immersion for 336 h. Probable mechanisms of zinc corrosion products formation are presented.

1. Introduction

Metallic materials have been widely applied for biomedical applications as orthopedic implants to restore lost functions [1,2]. It is well known that stainless steel 316 L [3,4], titanium and its alloys [5,6], and cobalt-based alloy [7,8] are common selection as metallic implant materials. However, these implants sometimes need to be removed under a secondary surgery after healing. Ideally, an orthopedic implant with acceptable mechanical properties could be biodegraded in accordance with the healing process. During the degradation process, the products are supposed to be non-toxic to human body and be gradually dissolved and absorbed.

Recently, zinc (Zn) and its alloys have attracted increasing attention as new biodegradable metals due to its biological merits, appropriate degradation rate and degradation behavior [9–11]. Zinc is an essential trace element in human physiology, which is widely acknowledged as an essential element for basic biological function [12]. The recommended dietary allowance (RDA) for Zn is 2 mg d^{-1} for infants, 11 mg d^{-1} for men and 8 mg d^{-1} for women [13]. Besides, Hennig et al. found that zinc exhibited a strong antiatherogenic property [14]. The biological merits of zinc meet the basic requirements for biodegradable metals. Mg and Fe have been considered as potential candidate materials for biodegradable metallic [15], while Mg and its alloys show high corrosion rate and are associated with evolution of hydrogen gas [16–18], Fe and its alloys corrode too slow and the corrosion products of which repel neighboring cells and biological matrix [19,20]. From a thermodynamic point of view, i.e. Mg (−2.37 V) < Zn (−0.763 V) < Fe (−0.440 V) (all V values vs. SHE), Zn has a standard electrode potential between Fe and Mg [21], which can theoretically predict that zinc provide intermediate corrosion rate in line with clinic demand.

Bowen et al. implanted pure zinc wires into the abdominal aorta of Sprague–Dawley rats, Zn degradation proceeds in rat arteries at a rate of 10–20 μm y^{-1}, nearly identical to the 20 μm y^{-1} benchmark value for ideal bioabsorbable materials [9]. Another in vivo test revealed that Zn exhibited good hemocompatibility and products of zinc corrosion may suppress the activities of inflammatory and smooth muscle cells [22]. Drelich et al. conducted clinically long term in vivo study, zinc wires implanted in the murine artery exhibited steady corrosion without local toxicity for up to at least 20 months postimplantation [23]. One *in vitro* evaluation showed that Zn exhibited non-cytotoxicity to endothelial cells [24]. Moreover, Chen et al. studied Zn, Fe and Mg in a long-term course of immersion in PBS solution to trace its dynamic degradation profile and the transient electrochemical results revealed

Peer review under responsibility of KeAi Communications Co., Ltd.
* Corresponding author. Beijing Advanced Innovation Center for Materials Genome Engineering, School of Materials Science and Engineering, University of Science and Technology Beijing, Beijing, 100083, China.
E-mail address: luning.wang@ustb.edu.cn (L.-N. Wang).

https://doi.org/10.1016/j.bioactmat.2018.08.003
Received 9 March 2018; Received in revised form 27 August 2018; Accepted 27 August 2018
Available online 11 October 2018

that the electrochemical potential and corrosion rate of Zn lied between Fe and Mg [25]. However the mechanical property of pure zinc is not allowed to apply in a biodegradable stent [13]. Mg, Cu, Mn and Li were selected as alloying elements to modify the mechanical properties and corrosion properties and the biocompatibility [26–29]. And These reports strongly implied the potential of Zn-based alloys to be used for biodegradable implants.

Corrosion behavior including the corrosion rate measurement and formation of corrosion products is crucial for understanding the basic corrosion processes underpinning absorption of biodegradable metals. By systematically examining the corrosion products formed on Zn, one may understand the evolution of the corrosion products during different immersion interval. Sodium, the major cation of the extracellular fluid, functions primarily in the control of water distribution, fluid balance, and osmotic pressure of body fluids. Chloride, the major extracellular anion, closely follows the metabolism of sodium. Many inorganic ions in physiological environments exert an important impact on the corrosion products of zinc. And the chloride ion is notorious for the corrosion of zinc alloys.

This paper reports the investigation of the corrosion behavior of pure zinc exposed to physiological saline solution (0.9% NaCl), which can be used to simulate the body environment [30].

2. Experimental

2.1. Electrochemical corrosion measurement

Zinc samples were cut into plates with the geometric sizes of 10 mm × 10 mm × 2 mm from 99.99% pure zinc ingot. The backside of the specimens was connected electrically with a copper wire and then was sealed with epoxy to expose the research surface (ca. 1 cm^2 area). Electrochemical corrosion measurements, including open circuit potential (OCP) vs. time, potentiodynamic polarization (PDP) and electrochemical impedance spectroscopy (EIS), were performed with an electrochemical workstation (ModuLab XM) at 37 ± 0.1 °C in 0.9% NaCl solution. A three-electrode set-up was used, containing a working electrode (the pure Zn samples), a reference electrode (saturated calomel electrode, SCE) and counter electrode (a platinum sheet, 1 cm × 1 cm). The potentiodynamic polarization (PDP) curves were carried out at a constant scan rate of 1 mV s^{-1}, initiating from −1.5 V_{SCE} to −0.7 V_{SCE}. The corrosion potential E_{corr}, corrosion current density I_{corr}, and cathodic Tafel slope were determined by the Tafel linear extrapolation. EIS studies were carried out in a frequency range from 100 kHz to 10 mHz at 10 mV sinusoidal amplitude of open circuit potential. The impedance data were analyzed with ZsimpWin3.5 software and fitted to the equivalent curves.

2.2. Immersion test

Samples were cut into 2 mm thick discs with 10 mm diameter. Prior to immersion, samples were mechanically grounded with silicon carbide sandpapers, then polished with diamond abrasive paste, followed by ultrasonically rinsed in milli-Q water, acetone and ethanol successively to remove surface contaminants. Then, the samples were dried and stored in a vacuum oven, prepared for further investigation.

Samples were immersed in 40 mL 0.9% NaCl (saline solution) at 37 ± 0.1 °C. The samples soaking up to 2 weeks (336 h) were taken out at different temporal intervals and investigated. During the immersion, the pH value of the saline solution was recorded by the FE 20 pH meter (Mettler Toledo). The amount of released Zn^{2+} in the saline solution was evaluated by atomic absorption spectrophotometer (AAS, Thermo Scientific M Series).

For different time interval, the corrosion products on the sample surfaces were removed in the chemical cleaning solution according to ISO 8407[31]: 100 g L^{-1} NH_4Cl for 2–5 min at 70 °C. Afterwards, the samples were rinsed by ethanol and dried before being weighted. The weight loss (mg cm^{-2}) was calculated using the following equation [32]:

$$Mass\ loss = \frac{m_i - m_f}{A} \quad (1)$$

where m_i is the initial weight of the sample before immersion (mg), m_f is the final weight of each sample after immersion (mg), A is the sample surface area exposed to r-SBF (cm^2). Also the corrosion rate (CR, mm y^{-1}) of pure Zn can be calculated by the following equation according to ASTM G31-72 [33]:

$$CR = 87.4 \times \frac{m_i - m_f}{A\ D\ t} \quad (2)$$

where m_i is the initial weight of the sample before immersion (in mg), m_f is the final weight of each sample after immersion (in mg), A is the exposed area (cm^2); D is the alloy density (in g cm^{-3}); t is the immersion time (in h).

2.3. Materials characterization

Surface morphology of Zn samples after immersion was investigated by a scanning electron microscope (SEM, FEI Quanta 200) coupled with an Oxford Instrument INCA X-max^N-sight EDX analyzer. X-ray photoelectron spectroscopy (PHI 5600 XPS spectrometer) was used to characterize the surface chemical states of samples after immersion. The XPS spectra were recorded using Al Kα radiation (1486.6 eV) as excitation source. The chemical groups of the corrosion products were characterized by Fourier transform infrared spectrometer (FTIR, Nicolet 5700) in the wave number ranging from 600 to 4000 cm^{-1}. X-ray diffraction (XRD) was conducted on the Smart Lab X-ray diffractometer (Rigaku) with Cu Kα radiation. The XRD spectra were collected at angles between 10° and 90° at a rate of 20° min^{-1}.

3. Results and discussion

3.1. Surface morphology

Fig. 1 portrays the surface of pure Zn taken from saline solution at different time during immersion. The samples still had metallic luster shortly after immersion up to 6 h (Fig. 1a). Then the metallic luster disappeared. Although there is severe corrosion sign on the samples immersed after 24 h and 48 h, it was because of the wire which hanged the samples to keep it vertical during the immersion. It is can be seen that localized whitish corrosion product appears on the sample surface after immersion up to 120 h. With the extension of immersion time, the corrosion products increased, which could be attributed to the corrosion products precipitated continuously during immersion (Fig. 1e and h).

Fig. 2 illustrates the corroded surface morphology of zinc after immersion for different periods and the inserts of each image show the magnified feature in the squared area. It can be seen that the surface keeps almost no change up to 48 h immersion with some grain boundary appearing (Fig. 2a and d). By observing the magnified feature, one can see that the nano-rods appear shortly after 6 h immersion on the surface. By extending the immersion time, the nano-rods covered the entire surface. The corrosion product showed clusters distribution after immersion in saline solution for 168 h (Fig. 2e). It also can be observed that there was a primary layer of corrosion products, over which further growth of the nano-rods cluster proceeded displaying in Fig. 2e and h. With prolonging the immersion time, the entire surface was covered by nano-rods and abundant clusters were deposited on top of the samples (Fig. 2e and h).

The degradation behavior of the zinc was elucidated by creating a series of cross sections from samples. SEM images and EDS profile in Fig. 3 were acquired from the cross-sectional observation and line-scan of Zn samples immersed for 120 h, 240 h and 336 h. It can be observed

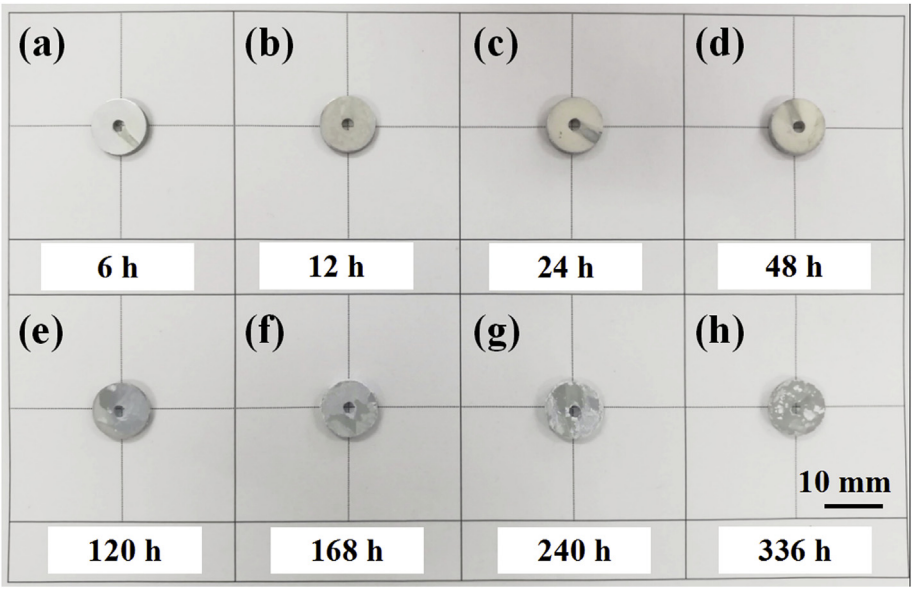

Fig. 1. Optical images of pure Zn tested in saline solution for different time.

that the thickness of the corrosion layer increased with the immersion time (Fig. 3a and c). A thin layer (ca. ~1.5 μm) was formed on the sample surface after immersion for 120 h (Fig. 3a). With the prolonging of immersion time to 240 h, a compact corrosion layer with thickness of ca. 3 μm was formed (Fig. 3b). The thickness of corrosion product reached a maximum value to 6 μm when the immersion time was prolonged to 336 h (Fig. 3c). And the surface after immersion 336 h was covered by rod-like corrosion products. According to the EDS line scan profiles, it can be observed that the corrosion product layer was mainly consisted of Zn, Cl and O (Fig. 3d and f). It can be seen that the intensity of Zn and O in the corrosion layer enhanced along with the immersion time. The O was enriched in the corrosion layer after immersion for 240 h and the intensity of O become quite stronger than the initial immersion time after 336 h, indicating that corrosion layer was mainly composed by oxygen-containing products.

3.2. XRD, XPS and FTIR analysis

Fig. 4 describes the XRD spectra of Zn immersed in saline solution for different time. In addition to the dominant peaks corresponding to Zn phase, the peak of ZnO appeared since the initial immersion stage and its intensity strengthened on the profile with the extension of immersion time, which became the dominant peak when the immersion time extended to 336 h. Number of peaks with relative low intensity for $Zn_5(OH)_8Cl_2{\cdot}H_2O$ were detected on the samples after immersion for 12 h. The peaks for this species also became stronger with the prolonging of time, which indicated the amount of $Zn_5(OH)_8Cl_2{\cdot}H_2O$ increasing in the corrosion products. The peaks for $Zn(OH)_2$ were only detected on the samples after immersion for 336 h, which could be attributed to their low contents that cannot be detected during the initial immersion stage. The results were coincident with the XPS data, clearly testifying the compositions of the corrosion products.

Fig. 5 shows the FTIR spectra of pure Zn sample immersed in saline solution for different time. Peaks at 1640 cm^{-1} were attributed to H_2O bending vibration [34] and rotation modes manifested the existence of crystal water [35]. The broad absorption from 3600 to 3100 cm^{-1} was attributed to the OH stretching bond [34]. The peak at 868 cm^{-1} was attributed to Zn-Cl [36]. It can be observed that Zn-Cl was hardly to be detected until after immersion for 120 h. And the intensity of Zn-Cl peak became stronger with the extension of time. The results indicated that more chlorides formed on Zn sample surfaces by extending the soaking time, which verified the presence of chloride species in the corrosion products. FTIR spectra on the species is well in agreement with the analysis retrieved from XRD results.

The set of samples which were immersed after 6 h, 48 h, 120 h, 240 h and 336 h were analyzed by means of XPS in order to evaluate the elemental and chemical compositions of and the results were shown in Fig. 6a. By analyzing the spectra, the corrosion product was mainly composed by Zn, O, Cl elements. There was no significant difference in elemental composition of the corrosion products after different immersion time. Corresponding high resolution spectra of Zn and Cl was collected in order to obtain detailed information about the corrosion products.

The Cl 2p spectra are depicted in Fig. 6b. There is only one chemical status of Cl 2p located at 198.8 eV, which is corresponding to $Zn_5(OH)_8Cl_2{\cdot}H_2O$ species [37]. The peak intensity increased significantly with the time prolonged, indicating that formation of $Zn_5(OH)_8Cl_2{\cdot}H_2O$ in surface is apparent after immersion for longer time. The Zn-$2p_{3/2}$ spectra are depicted in Fig. 6c. The deconvoluted spectra clearly demonstrated the composition of the corrosion products with the prolonging of immersion time. There were two chemical status when the pure zinc immersed after different times, $ZnO/Zn(OH)_2$ located at 1022.26 eV [38] and $Zn_5(OH)_8Cl_2{\cdot}H_2O$ located at 1021.8 eV [37](Fig. 6d-g). With the extension of immersion time, the proportion of $Zn_5(OH)_8Cl_2{\cdot}H_2O$ in the corrosion product increased when the immersion time extended. The result of Zn $2p_{3/2}$ showed the same trend of corrosion products as Cl 2p and confirmed the presence of $Zn_5(OH)_8Cl_2{\cdot}H_2O/ZnO$ and $Zn(OH)_2$ in corrosion products.

According to the results from FTIR, XPS and XRD, it is confirmed that the predominant components of the corrosion products were zinc oxides (ZnO), zinc hydroxide ($Zn(OH)_2$) and zinc hydroxide chloride ($Zn_5(OH)_8Cl_2{\cdot}H_2O$). With the immersion time increased, corrosion products precipitated continuously on the surfaces.

3.3. pH assessment, dissolution and weight loss test

pH values of the saline solution during zinc immersion as a function of immersion time is shown in Fig. 7a. The pH value increased monotonically with extended time and reached 7.61 after 336 h immersion, owing to the base corrosion reactions of producing OH^- anion. Although the increasing tendency of the pH value were different before and after immersion in 120 h, the value generally changed mildly, which could not induce much change to the surrounding culture. Fig. 7b shows the accumulated Zn^{2+} ion of immersed Zn samples as a

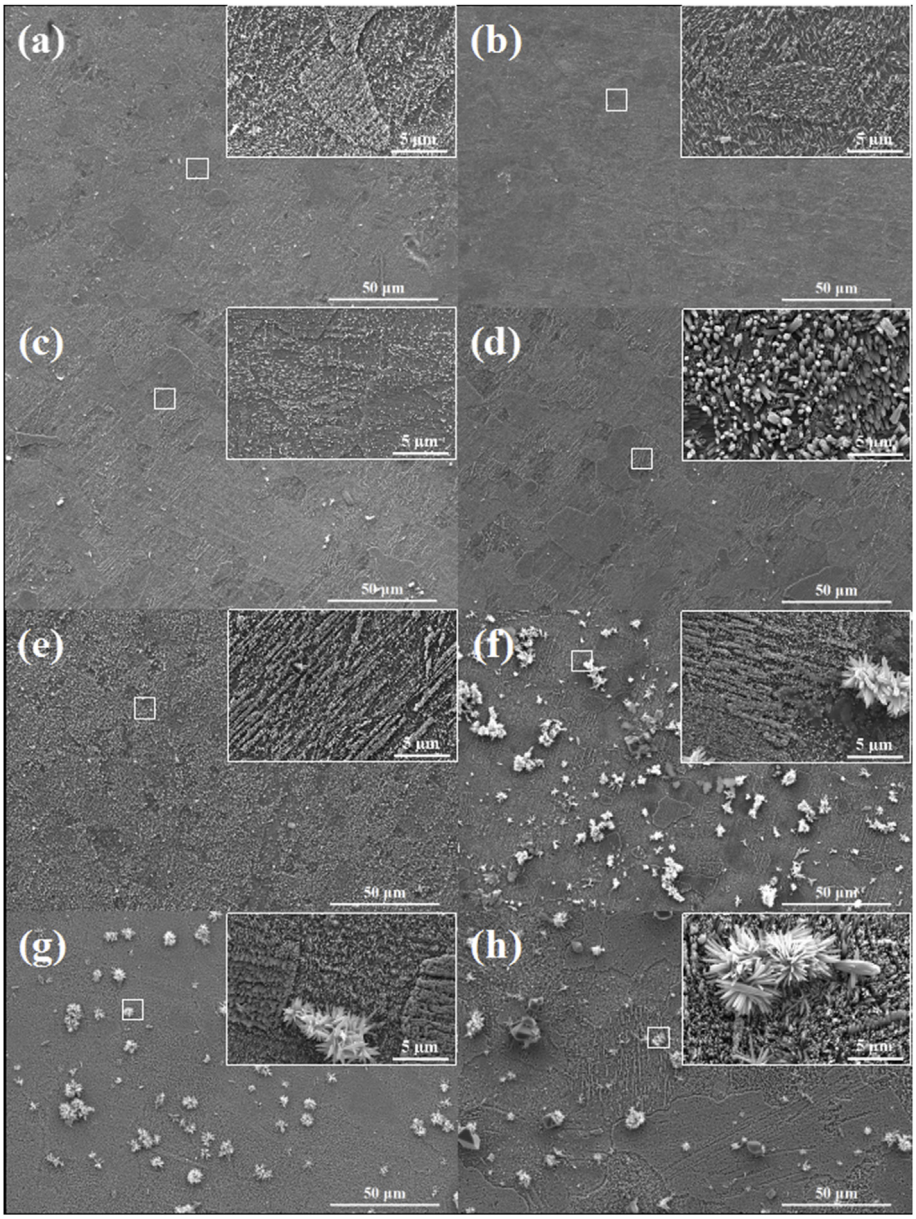

Fig. 2. SEM images of pure Zn immersed in saline solution for (a) 6 h, (b) 12 h, (c) 24 h, (d) 48 h, (e) 120 h, (f) 168 h, (g) 240 h and (h) 336 h. The insets show the magnified feature in the squared area.

function of immersion time. It was obvious that the dissolution of Zn took place consistently as the time prolonged. The release rate of Zn^{2+} increased after 120 h immersion, which was in accordance with the trend of weight loss (Fig. 7c). The slow increase of pH value is likely because of the consumption of products and less generation of OH^-, as shown in XRD profile that there were more $Zn(OH)_2$ and $Zn_5(OH)_8Cl_2{\cdot}H_2O$ formed after relatively longer time immersion than those formed at initial stage. Besides, Yadav et al. [39] mentioned that reduction of oxygen was inhibited when there was a thick corrosion layer on zinc, which may reduce the dissolution rate of Zn^{2+}. After 336 h, the accumulated release Zn^{2+} was about 210 mg L^{-1}. Thus, the average Zn^{2+} release rate was about 0.03 mg cm^{-2} d^{-1}. And according to equation (2), the CR of Zn after immersion for 336 h was about 0.063 mm y^{-1}.

3.4. Micrograph of corroded Zn sample

Fig. 8 shows optical images of pure Zn samples after soaking in saline solution and removing the corrosion product in order to unveil the underneath corrosion attack. The top view showed uniform corrosion on zinc. Corrosion attack and products formation that undertook homogenously on the whole surface. However, it seems that some voids could be observed (Fig. 8b and c), indicating a tendency of localized corrosion after immersion in saline solution. Boshkov et al. [40] reported that chloride ions (Cl^-) participated in the reaction to form zinc hydroxide chloride in the pits and their neighborhood areas. And the localized corrosion in saline solution was in accordance with some research about the *in vitro* test of Zn. Cheng et al. [21] reported that pure Zn was attacked under localized corrosion in Hank's solution; and Chen et al. [24] reported that Zn presented apparently cavity/hole- and groove-like morphology underneath the product layer after immersion in PBS for 21 d. Our results confirmed that pure Zn may encounter localized corrosion after immersion in Cl^- containing solution. Thus, pure Zn may not be a promising material for practical application. However, alloy design may be a promising approach to enhance the localized corrosion resistance of zinc.

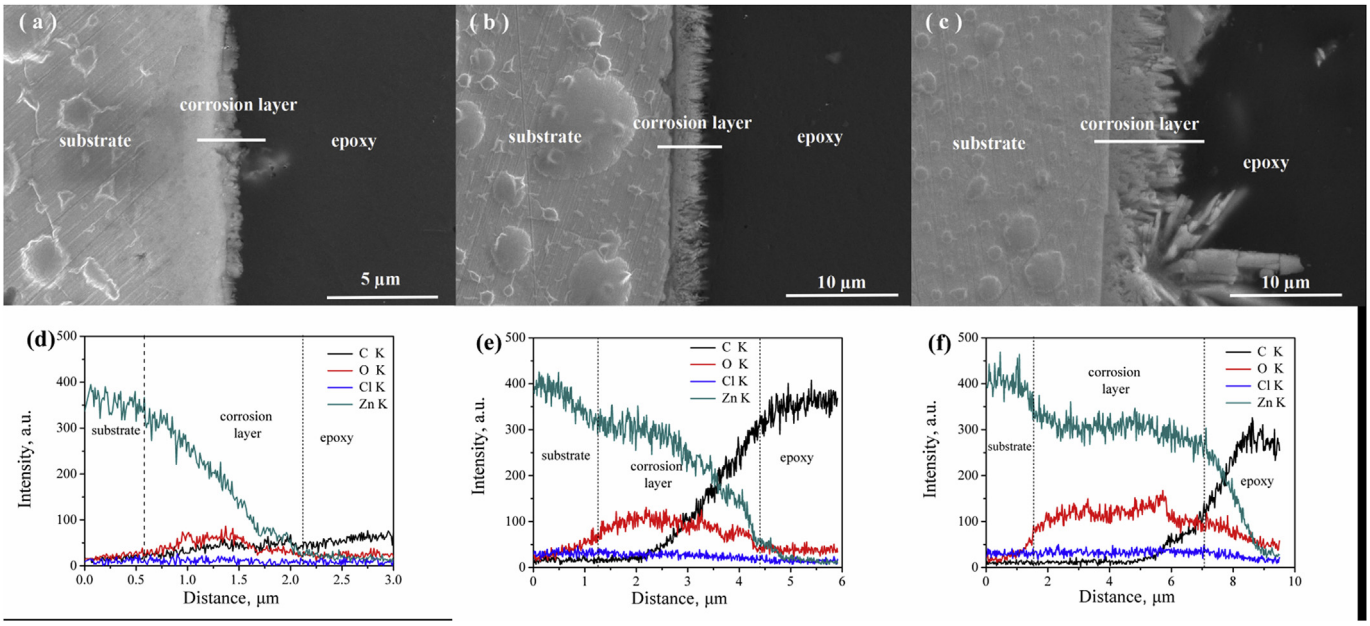

Fig. 3. Cross-sectional images and EDS line profile of pure Zn immersed in saline solution for (a, c) 120 h, (b, d) 240 h, (c, f) 336 h.

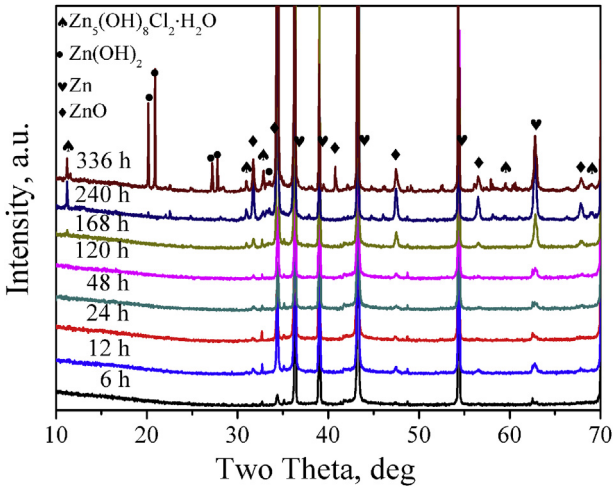

Fig. 4. XRD patterns of Zn after immersion in saline solution for different time.

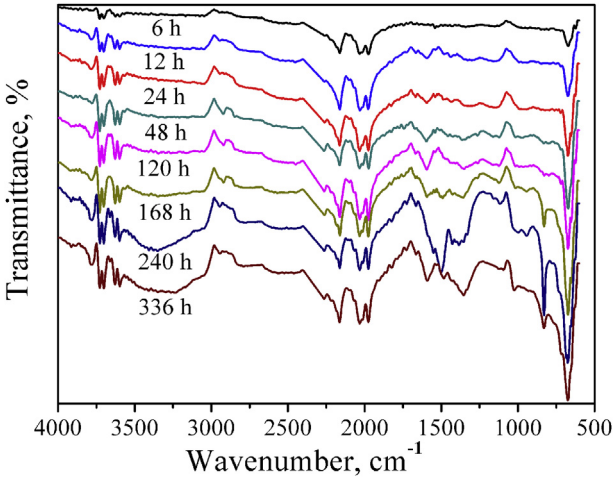

Fig. 5. FTIR spectra of Zn after immersion in saline solution for different time.

3.5. Potentiodynamic polarization measurements

Fig. 9a portrays the potentiodynamic polarization (PDP) curves of pure Zn soaking in saline solution up to 48 h. These curves can be divided into several potential domains. The cathodic domain includes potential below −1.15 V_{SCE} for all the curves. At potential below −1.3 V_{SCE}, the near vertical stage of current density mainly corresponds to hydrogen generation process (Eq. (3)), whereas the slope region (mainly from −1.3 V_{SCE} to −1.2 V_{SCE}) represents the oxygen consumption process (Eq. (4) and 5).

$$2H_2O + 2e^- \rightarrow 2OH^- + H_2 \quad (3)$$

$$O_2 + H_2O + 2e^- \rightarrow HO_2^- + OH^- \quad (4)$$

$$HO_2^- + H_2O + 2e^- \rightarrow 3OH^- \quad (3)$$

The peaks at ~ -1.2 V_{SCE} in the cathodic branch of the PDP curves likely correspond to the mixed potential of the hydrogen evolution reaction and the anodic dissolution [41,42]. At relative higher potentials, the hydrogen evolution reaction was suppressed. Thus the peaks at −1.1 ~ −1.0 V_{SCE} refer to the mixed potential of oxygen reduction reaction and anodic dissolution. As the immersion time increased, the formation of corrosion product film on the zinc surface hindered the oxygen diffusion [39]. As a result, the cathodic reaction was dominated by hydrogen evolution (it was observed that the peak at cathodic branch on sample immersed for 48 h almost diminished). The anodic branches of samples immersed up to 48 h show only acceleration of anodic dissolution, implying that there is no stable corrosion product formed during the immersion at this stage.

Fig. 9b portrays the PDP curves of sample after being immersed in saline solution from 120 h to 336 h. It is apparent that all the cathodic branch experiences mixed oxygen reduction reactions and hydrogen evolution reaction. Because the corrosion product at this time stage is thicker than that immersion at 48 h, no significant dissolution peaks could be found at cathodic branch. The anodic branches in all curves performed an obvious passive plateau until a passivity broken down owing to dissolution of corrosion products and the substrate under high potential. There is a decrease of anodic current density, passive potential as well as passive current density, demonstrating the intrinsic character of the corrosion product during different immersion time. It implies that the corrosion product formed at 120 h was relatively dense. By increasing the immersion time from 168 h to 336 h, the film of corrosion product became heterogenous and loosening from the

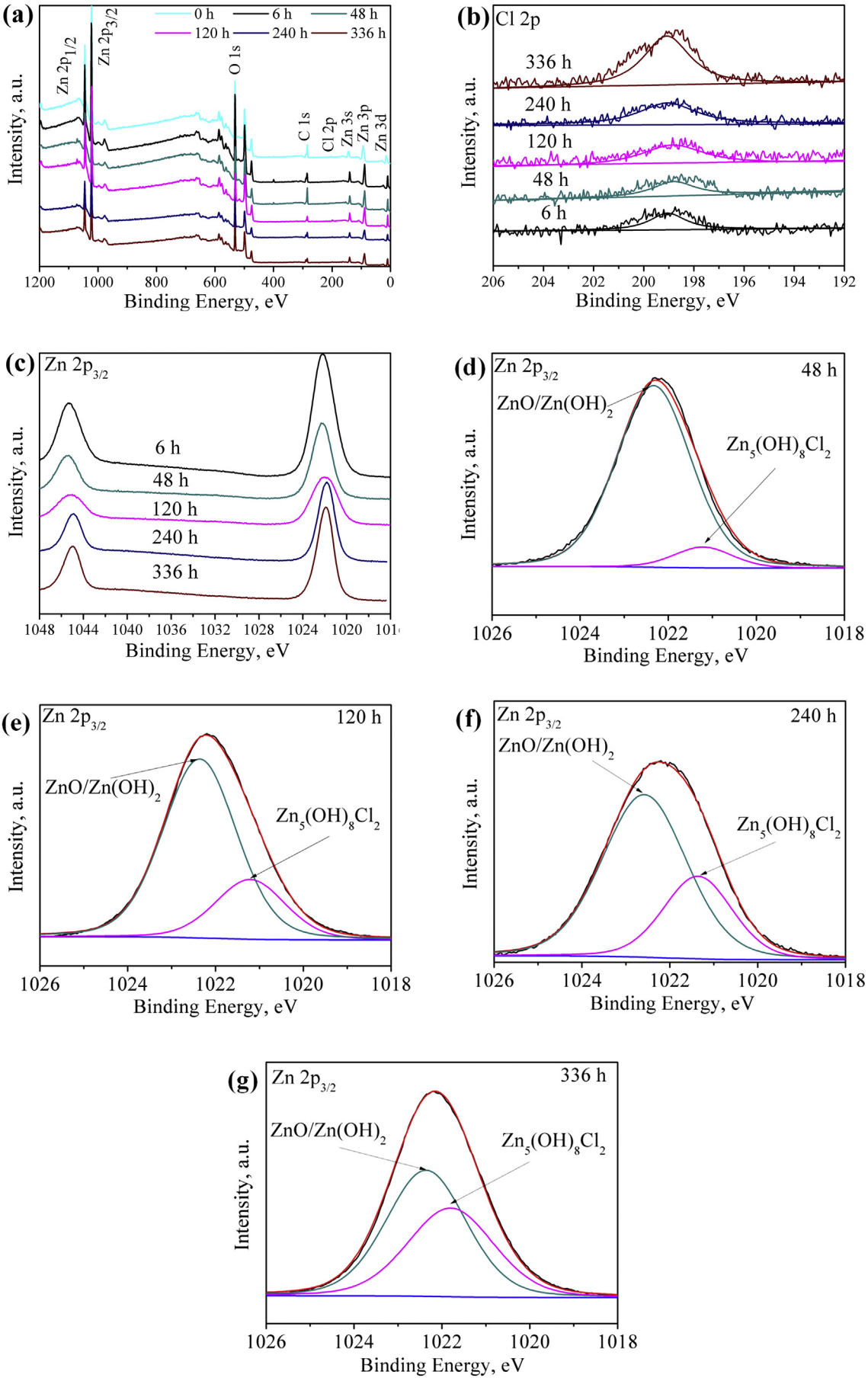

(caption on next page)

Fig. 6. XPS spectra of pure Zn: (a) The overview XPS spectrum, (b) Cl 2p and (c) Zn 2p3/2 spectra of pure Zn after immersion in saline solution for 6 h, 12 h, 24 h, 48 h, 120 h, 168 h, 240 h and 336 h; Deconvoluted XPS spectra (d–g) of Zn 2p3/2 after immersion for 48 h, 120 h, 240 h and 336 h.

substrate. This phenomenon demonstrates that the corrosion product formed after 120 h immersion may play a protective role for the substrate. It was reported that zinc showed passive behavior of zinc in NaCl solution attributed to the formation of zinc hydroxide and zinc oxide [43]. According to the XRD results, there were a great quantity of zinc hydroxide and zinc oxide on surface after immersion, which led to the passivation behavior. However, by extending the immersion time, the intrinsic dissolution character of the corrosion products could be revealed.

Fig. 9c summarized the value of E_{corr} and current density with respect to the immersion time. It is found that the value of E_{corr} decreases with the increasing of immersion time up to 120 h (Fig. 9c). Then the value of E_{corr} keeps almost constantly, indicating a stable tendency for long term degradation. The cathodic polarization curves were picked for current density (i_{corr}) of Zn by using linear extrapolation, which is reliable for active metals. As immersion progressed, the i_{corr} of Zn increased from 5 μA cm^{-2} at the initial stage to ~16 μA cm^{-2} after 336 h immersion, which is due to the formation of zinc hydroxide chloride.

EIS analysis between 10^{-2} and 10^{5} Hz with amplitude of 10 mV at the open circuit potential condition was performed on Zn after immersion from 0 to 336 h in saline solution to investigate the influence of immersion on the electrode/electrolyte interface. Fig. 10 shows a series of EIS plots of Zn immersed for different time. The Nyquist plots of sample immersed for up to 48 h was performed in Fig. 10a. It was observed two capacitive loops in Nyquist plots. Meanwhile, two peaks were also found in the Bode plots, representing two time constants. It is acknowledged that a large diameter of the capacitive loop in the Nyquist plots represents a high corrosion resistance of the working electrode [37]. The two loops likely indicated that the corrosion product might contain two distinct layers, a relative dense one and another porous one. It is obvious that the diameter of first capacitive loop increased during the first 48 h, due to the gradually formation of corrosion products to protect the surface. Fig. 10b portrays the Nyquist plot of samples immersed from 120 h to 336 h. The second capacitive loops began to diminish and merged with the first one with the extension of immersion time. There was only one apparent loop for sample immersed for 336 h, indicating the corrosion product might merge to one layer.

The fitted models (a) {Rs (Q_1R_1) (Q_2R_2)} and (b){Rs (Q_1 (R_1 (Q_2R_2)))} in Fig. 10 gave satisfactory results to EIS. The model{Rs (Q_1R_1) (Q_2R_2)} was used for the immersion during 48 h and the model {Rs (Q_1 (R_1 (Q_2R_2)))}was used to immersion after 120 h. Both fitted parameters were summarized in Table 1. R_1 corresponds to a charge-transfer resistance and R_2 is due to the adsorbed species that contribute to the formation of the corrosion layer. The R_1 value increased during 48 h and then decreased, the small charge-transfer resistance was due to oxidation of zinc electrode was inhibited by the corrosion products. The corrosion layer covered the whole surface of zinc electrode and its thickness also grew consequently, which was the same as shown at the cross section SEM. Q is used in place of a capacitor to compensate for the non-homogeneity of system [44]. As reported by Heakal [45], the total resistance value R_t, given by $R_t = R_1 + R_2$, which was equal to the charge-transfer resistance. The highest R_t value appeared at 48 h, which was in accordance with i_{corr}.

3.6. Mechanism of zinc corrosion in saline solution

According to the results interpreted in previous sections, the main corrosion products on zinc during immersion in saline solution are zinc oxide, zinc hydroxide and zinc hydroxide chloride. The chemical reaction process may contain the following steps [39,42,46]:

Initially, pure Zn dissolved from onset of immersion via the chemical reaction

$$Zn \rightarrow Zn^{2+} + 2e^{-} \quad (4)$$

Meanwhile, oxygen reduction carried out near the zinc surface.

$$O_2 + H_2O + 2e^{-} \rightarrow 4OH^{-} \quad (5)$$

The reaction (7) leaded to a local increase in pH value in the depth

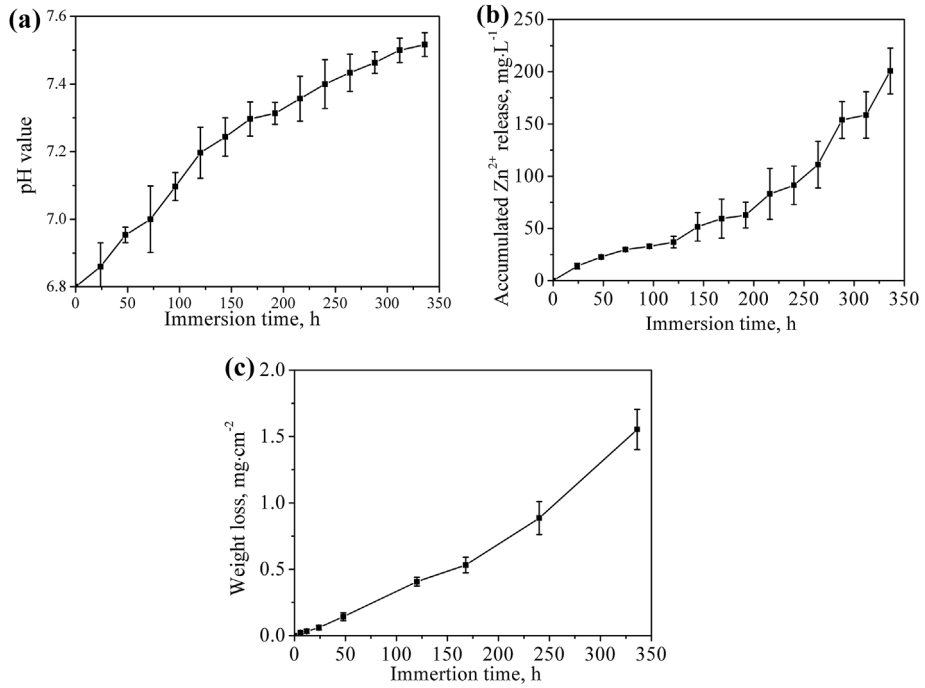

Fig. 7. (A) pH vibration in saline solution, (b) accumulated Zn^{2+} ion and (c) weight loss vibration of immersed Zn samples as a function of immersion time.

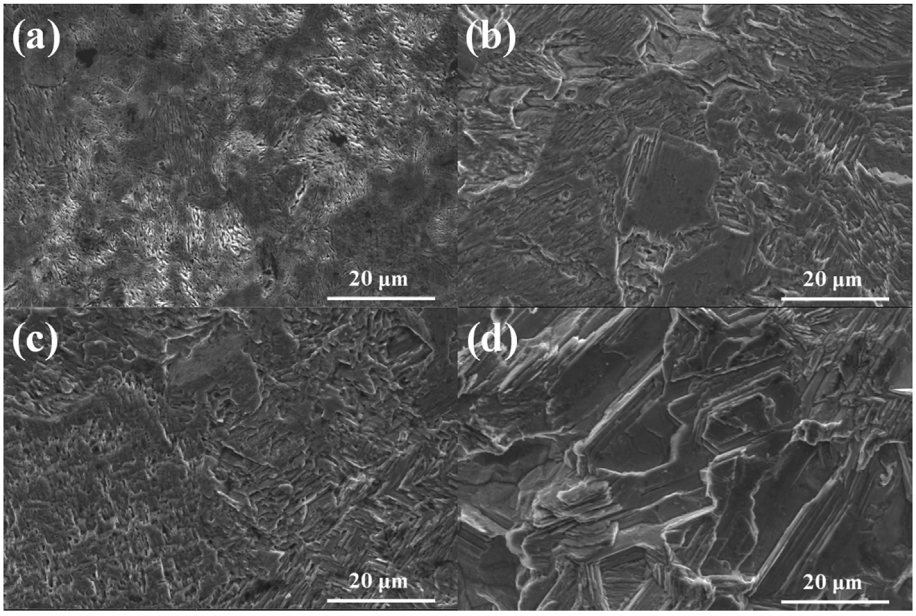

Fig. 8. SEM images of Zn samples after immersed in saline solution and removal of corrosion product: (a) 48 h, (b) 120 h, (c) 240 h and (d) 336 h.

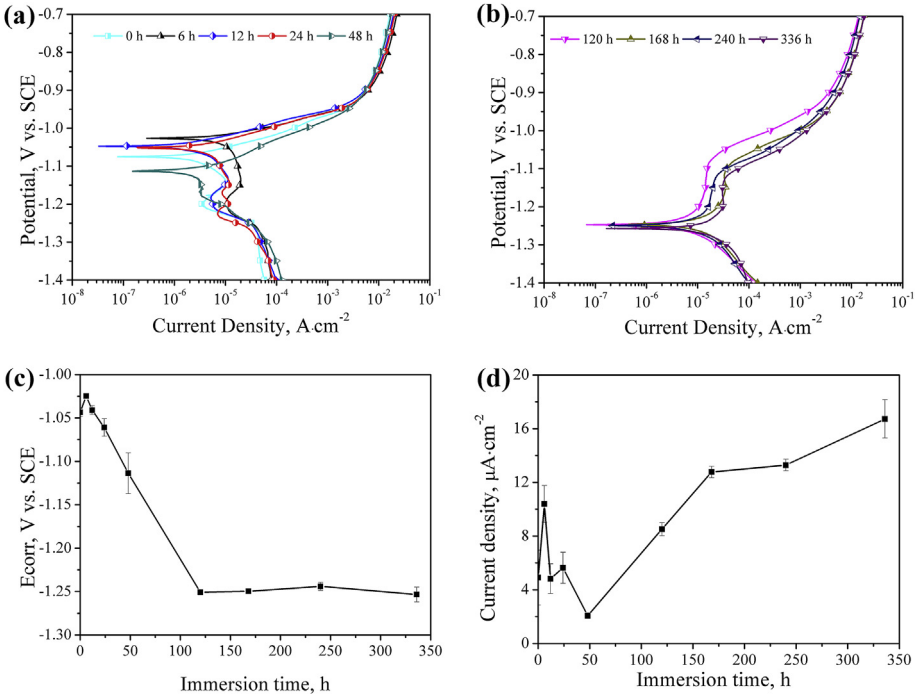

Fig. 9. Potentiodynamic polarization curves of pure Zn at different immersion periods in saline solution. (a) 0 h, 6 h, 12 h, 24 h, 48 h, (b) 120 h, 168 h, 240 h and 336 h. (c) The value of E_{corr} with respect to the immersion time. (d) The value of current density with respect to the immersion time.

of the corrosion damages.

And Zn^{2+} ions from the substrate can react with OH^- to form $Zn(OH)_2$, parts of which can be dehydrated to form ZnO.

$$Zn^{2+} + 2OH^- \rightarrow Zn(OH)_2 \quad (8)\ Zn(OH)_2 \rightarrow ZnO + H_2O \qquad (6)$$

With the immersion time extended to 48 h (Fig. 11a), that maturing and thickening of the accumulated $Zn(OH)_2$/ZnO layer on the samples contributed to the inhibition of Zn dissolution, the whole surface of samples were nearly covered with corrosion products, which caused the lowest i_{corr}. With the reaction constantly happened, the pH value increased, when the pH was high enough, Part of $Zn(OH)_2$ would react with OH^- to form $Zn(OH)_4^{2-}$, so the pH value may increase slowly after 48 h, just as discussed previously.

$$Zn(OH)_2 + 2OH^- \rightarrow Zn(OH)_4^{2-} \qquad (7)$$

In the presence of chloride ions (Cl^-), the following chemical reaction occurred and Zinc chloride hydroxide is formed:

$$5Zn^{2+} + 8OH^- + 2\ Cl^- + H_2O \rightarrow Zn_5(OH)_8Cl_2{\cdot}H_2O \qquad (8)$$

The $Zn(OH)_2$ could also be the precursor of Zinc chloride hydroxide. So the following chemical reaction happened:

$$5Zn(OH)_2 + 2\ Cl^- + H_2O \rightarrow Zn_5(OH)_8Cl_2{\cdot}H_2O + 2OH^- \qquad (9)$$

The reaction (11) and (12) mainly occurred after 120 h immersion

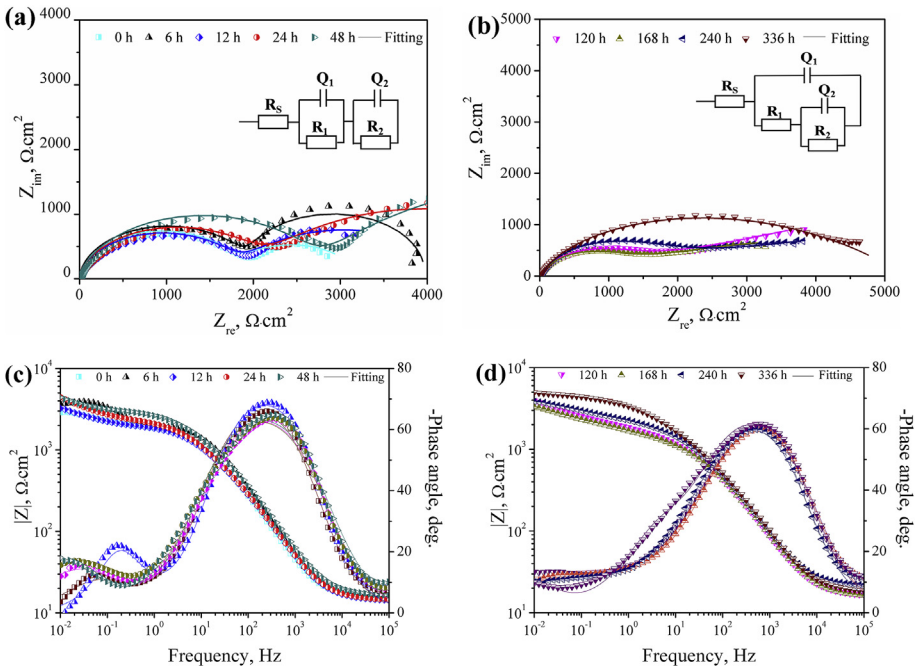

Fig. 10. EIS data of pure Zn after immersion in saline solution: (a) (b) Nyquist plots and equivalent circuit models. (c) (d) Bode plots of |Z| vs. frequency and phase angle vs. frequency. Different immersion periods: (a,c) 0 h, 6 h, 12 h, 24 h, 48 h (b,d)120 h, 168 h, 240 h, 336 h. Symbols represent experimental data and lines represent simulated spectra.

Table 1
Equivalent electrical circuit parameters of the pure Zn at different immersion periods in saline solution.

Immersion time	R_s (Ω cm^2)	Q_1 ($\mu\Omega^{-1}$ s^{-1} cm^{-2})	n	R_1 (Ω cm^2)	R_2 (Ω cm^2)	Q_2 ($\mu\Omega^{-1}$ s^{-1} cm^{-2})
0 h	15.2 ± 0.4	(1.8 ± 0.2) × 10^{-5}	0.82 ± 0.02	1380 ± 160	1780 ± 100	(1.7 ± 0.1) × 10^{-5}
6 h	15.5 ± 0.6	(1.1 ± 0.1) × 10^{-5}	0.84 ± 0.05	1880 ± 60	1810 ± 80	(1.7 ± 0.4) × 10^{-5}
12 h	13.5 ± 1.4	(1.4 ± 0.2) × 10^{-5}	0.76 ± 0.04	2510 ± 80	2020 ± 280	(2.2 ± 0.6) × 10^{-5}
24 h	13.6 ± 0.5	(1.8 ± 0.5) × 10^{-5}	0.79 ± 0.01	2680 ± 90	2110 ± 170	(2.3 ± 0.1) × 10^{-5}
48 h	15.2 ± 0.3	(2.1 ± 0.8) × 10^{-5}	0.77 ± 0.01	3850 ± 250	5790 ± 360	(2.0 ± 0.8) × 10^{-5}
120 h	15.6 ± 1.2	(1.0 ± 0.1) × 10^{-5}	0.81 ± 0.07	530 ± 180	6270 ± 140	(5.2 ± 0.7) × 10^{-4}
168 h	15.4 ± 0.6	(1.1 ± 0.4) × 10^{-5}	0.81 ± 0.03	780 ± 40	7000 ± 550	(5.5 ± 0.8) × 10^{-4}
240 h	15.0 ± 0.8	(1.0 ± 0.4) × 10^{-5}	0.80 ± 0.06	1150 ± 170	5260 ± 350	(8.9 ± 2.2) × 10^{-4}
336 h	14.8 ± 0.5	(0.8 ± 0.2) × 10^{-5}	0.84 ± 0.02	1230 ± 130	4650 ± 210	(4.2 ± 1.0) × 10^{-4}

(Fig. 11b). the increase in pH can promote more formation of corrosion product ($Zn_5(OH)_8Cl_2{\cdot}H_2O$) around the pits and their neighborhood areas in neutral Cl^- containing solution, which were caused by reaction (7). But the main reaction was still to form ZnO and $Zn(OH)_2$ to contribute the thickness of oxide films. The Sites of $Zn_5(OH)_8Cl_2{\cdot}H_2O$ products can be regarded as relative severe local corrosion sites, which accelerated the corrosion rate after 48 h. In any case, the oxide film's characteristics control the rate of diffusion of zinc ions [47] and oxygen and affect corrosion rate.

4. Conclusions

The initial corrosion behavior and corrosion products of pure Zn in saline solution have been investigated to trace details regarding the degradation profile. It is thought that this fundamental understanding of degradation studies is of utmost importance for research on biodegradation of Zn-based materials. Following conclusions can be drawn:

1 The pure Zn displayed uniform corrosion and homogeneous-distributed corrosion products on surfaces during the immersion for 336 h.
2 The initial corrosion products formed on pure Zn mainly consisted of

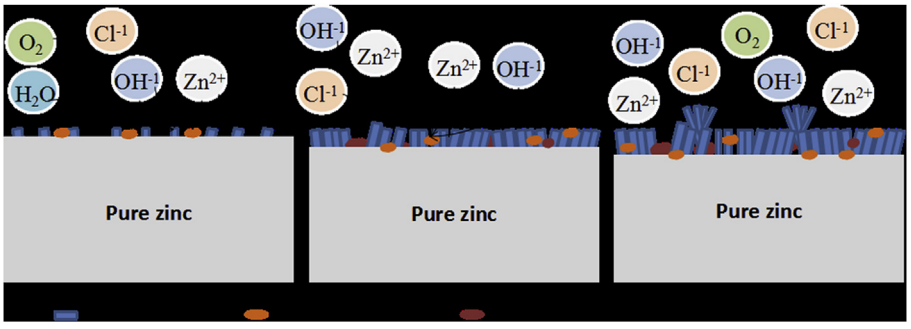

Fig. 11. Schematic illustration of corrosion process of pure Zn immersed saline solution.

ZnO, $Zn(OH)_2$ and $Zn_5(OH)_8Cl_2{\cdot}H_2O$. And the proportion $Zn_5(OH)_8Cl_2{\cdot}H_2O$ increased with time prolonged.

3 The degradation of Zn in saline solution didn't lead to much change to the surrounding culture.

4 The passivation of zinc occurred after 120 h immersion due to the stable corrosion products and the corrosion rate increased after 120 h.

Acknowledgements

Authors are grateful for the National Key R&D Program of China (Grant No. 2016YFC1102500), National Natural Science Foundation of China (Grant No. 51503014 and No. 51501008) and financial support from the State Key Laboratory for Advanced Metals and Materials (No. 2016Z-03).

References

[1] L. Xuan, C. Chu, P.K. Chu, Effects of external stress on biodegradable orthopedic materials: a review, Bioactive. Mater. 1 (2016) 77–84.
[2] Y.P. Kathuria, Laser microprocessing of metallic stent for medical therapy, J. Mater. Process. Technol. 170 (2005) 545–550.
[3] C.C. Shih, S.K.Y. Chou, Stability of passivated 316L stainless steel oxide films for cardiovascular stents, J. Biomed. Mater. Res. a. 80 (2007) 861–873.
[4] H. Zhao, H.J. Van, J. Sohier, S. De, Electrochemical polishing of 316L stainless steel slotted tube coronary stents, J. Mater. Sci. Mater. Med. 13 (2002) 911–916.
[5] Y. Li, K.S. Munir, J. Lin, C. Wen, Titanium-niobium pentoxide composites for biomedical applications, Bioact. Mater. 1 (2016) 127–131.
[6] X. Liu, P.K. Chu, C. Ding, Surface modification of titanium, titanium alloys, and related materials for biomedical applications, Mater. Sci. Eng. R. 47 (2004) 49–121.
[7] J.A. Disegi, R.L. Kennedy, R. Pilliar, Cobalt-base Alloys for Biomedical Applications, ASTM, 1999.
[8] Y. Bao, K.M. Krishnan, Preparation of functionalized and gold-coated cobalt nanocrystals for biomedical applications, J. Magn. Magn Mater. 293 (2005) 15–19.
[9] P.K. Bowen, J. Drelich, J. Goldman, Zinc exhibits ideal physiological corrosion behavior for bioabsorbable stents, Adv. Mater. 25 (2013) 2577–2582.
[10] A. Purnama, H. Hermawan, D. Mantovani, Biodegradable metal stents: a focused review on materials and clinical studies, J. Biomater. Tiss. Eng. 4 (2014) 868–874.
[11] H. Li, Y. Zheng, L. Qin, Progress of biodegradable metals, Prog. Nat. Sci.: Met. Mater. Int. 24 (2014) 414–422.
[12] C.J. Frederickson, J.Y. Koh, A.I. Bush, The neurobiology of zinc in health and disease, Nat. Rev. Neurosci. 6 (2005) 449–462.
[13] P.K. Bowen, E.R. Shearier, S. Zhao, Biodegradable metals for cardiovascular stents: from clinical concerns to recent Zn - alloys, Adv. Healthc. Mater. 5 (2016) 1121–1140.
[14] B. Hennig, M. Toborek, C.J. Mcclain, Antiatherogenic properties of zinc: implications in endothelial cell metabolism, Nutr. 12 (1996) 711–717.
[15] M. Moravej, D. Mantovani, Biodegradable metals for cardiovascular stent application: interests and new opportunities, Int. J. Mol. Sci. 12 (2011) 4250–4270.
[16] J. Kuhlmann, I. Bartsch, E. Willbold, et al., Fast escape of hydrogen from gas cavities around corroding magnesium implants, Acta Biomater. 9 (2013) 8714–8721.
[17] M.P. Staiger, A.M. Pietak, J. Huadmai, et al., Magnesium and its alloys as orthopedic biomaterials: a review, Biomaterials 27 (2006) 1728–1734.
[18] J. Chen, L. Tan, K. Yang, Effect of heat treatment on mechanical and biodegradable properties of an extruded ZK60 alloy, Bioact. Mater. 1 (2016) 19–26.
[19] M. Schinhamme, A.C. Hänzi, J.F. Löffler, P.J. Uggowitzer, Design strategy for biodegradable Fe-based alloys for medical applications, Acta Biomater. 6 (2010) 1705–1713.
[20] M. Schinhammer, Development and characterization of biodegradable Fe-based alloys for temporary medical applications, Dry. Technol. 28 (2012) 380–388.
[21] J. Cheng, B. Liu, Y.H. Wu, Y.F. Zheng, Comparative in vitro study on pure metals (Fe, Mn, Mg, Zn and W) as biodegradable metals, J. Mater. Sci. Technol. 29 (2013) 619–627.
[22] P.K. Bowen, G.R. Nd, E.R. Shearier, J.M. Seitz, J. Drelich, Metallic zinc exhibits optimal biocompatibility for bioabsorbable endovascular stents, Mater. Sci. Eng. C Mater. Biolo. Appl. 56 (2015) 467–472.
[23] A.J. Drelich, R.J. Guillory II, J.W. Drelich, J. Goldman, Long-term surveillance of zinc implant in murine artery: surprisingly steady biocorrosion rate, Acta Biomater. 58 (2017) 539–549.
[24] E.R. Shearier, P.K. Bowen, W. He, A. Drelich, J. Drelich, Adhesion, and proliferation of human vascular cells exposed to zinc, ACS Biomater. Sci. Eng. 2 (2016) 634–642.
[25] Y. Chen, W. Zhang, M.F. Maitz, et al., Comparative corrosion behavior of Zn with Fe and Mg in the course of immersion degradation in phosphate buffered saline, Corrosion Sci. 111 (2016) 541–555.
[26] Z. Tang, H. Huang, J. Niu, et al., Design and characterizations of novel biodegradable Zn-Cu-Mg alloys for potential biodegradable implants, Mater. Des. 117 (2017) 84–94.
[27] J. Niu, Z. Tang, H. Hua, et al., Research on a Zn-Cu alloy as a biodegradable material for potential vascular stents application, Mater. Sci. Eng. C 69 (2016) 407–413.
[28] S. Zhao, J.M. Seitz, R. Eifler, et al., Zn-Li alloy after extrusion and drawing: structural, mechanical characterization, and biodegradation in abdominal aorta of rat, Mater. Sci. Eng. C Mater. Biol. Appl. 76 (2017) 301–312.
[29] S. Zhao, C.T. Mcnamara, P.K. Bowen, et al., Structural characteristics and in vitro, biodegradation of a novel Zn-Li alloy prepared by induction melting and hot rolling, Metall. Mater. Trans. 48 (2017) 1204–1215.
[30] S. Awad, S.P. Allison, D.N. Lobo, The history of 0.9% saline, Clin. Nutr. 27 (2008) 179–188.
[31] ISO 8407:2009 (E), Corrosion of Metals and Alloys-Removal of Corrosion Products from Corrosion Test Specimens, International Standard ISO 8407, second ed., (2009).
[32] H. Ibrahim, A.D. Klarner, B. Poorganji, et al., Microstructural, mechanical and corrosion characteristics of heat-treated Mg-1.2Zn-0.5Ca (wt%) alloy for use as resorbable bone fixation material, J. Mec. Behav. Biomed. Mater. 69 (2017) 203–212.
[33] ASTM, Standard Practice for Preparing, Cleaning, and Evaluating Corrosion Test Specimens, ASTM Standard G1-03. 2011 Annual Book of ASTM Standards 03.02 ASTM, Philadelphia. PA, 2011.
[34] R.C. Zeng, X.T. Li, L.J. Liu, et al., In vitro degradation of pure Mg for esophageal stent in artificial saliva, J. Mater. Sci. Technol. 32 (2016) 437–444.
[35] K. Li, B. Wang, B. Yan, et al., Microstructure, in vitro corrosion and cytotoxicity of Ca-P coatings on ZK60 magnesium alloy prepared by simple chemical conversion and heat treatment, J. Biomater. Appl. 28 (2013) 375–384.
[36] K.M. Parida, L. Mohapatra, Carbonate intercalated Zn/Fe layered double hydroxide: a novel photocatalyst for the enhanced photo degradation of azo dyes, Chem. Eng. J. 179 (2012) 131–139.
[37] J. Duchoslav, R. Steinberger, M. Arndt, et al., Evolution of the surface chemistry of hot dip galvanized Zn–Mg–Al and Zn coatings on steel during short term exposure to sodium chloride containing environments, Corrosion Sci. 91 (2015) 311–320.
[38] B. Ramezanzadeh, H. Vakili, R. Amini, The effects of addition of poly(vinyl) alcohol (PVA) as a green corrosion inhibitor to the phosphate conversion coating on the anticorrosion and adhesion properties of the epoxy coating on the steel substrate, Appl. Surf. Sci. 327 (2015) 174–181.
[39] A.P. Yadav, A. Nishikata, T. Tsuru, Oxygen reduction mechanism on corroded zinc, J. Electroanal. Chem. 585 (2005) 142–149.
[40] N. Boshkov, K. Petrov, S. Vitkova, et al., Composition of the corrosion products of galvanic alloys Zn-Co and their influence on the protective ability, Surf. Coating. Technol. 157 (2002) 171–178.
[41] B.R.W. Hinton, L. Wilson, The corrosion inhibition of zinc with cerous chloride, Corrosion Sci. 29 (1989) 967–975 977-985.
[42] Z.F. Lodhi, J.M.C. Mol, A. Hovestad, et al., Corrosion resistance of Zn–Co–Fe alloy coatings on high strength steel, Surf. Coating. Technol. 203 (2009) 1415–1422.
[43] M. Mouanga, P. Berçot, Comparison of corrosion behaviour of zinc in NaCl and in NaOH solutions; Part II: electrochemical analyses, Corrosion Sci. 52 (2010) 3993–4000.
[44] L. Liu, P. Li, Y. Zou, K. Luo, et al., In vitro corrosion and antibacterial performance of polysiloxane and poly(acrylic acid)/gentamicin sulfate composite coatings on AZ31 alloy, Surf. Coating. Technol. 291 (2016) 7–14.
[45] Y. Song, D. Shan, R. Chen, E.H. Han, Corrosion characterization of Mg–8Li alloy in NaCl solution, Corrosion Sci. 51 (2009) 1087–1094.
[46] M. Mouanga, P. Berçot, J.Y. Rauch, Comparison of corrosion behaviour of zinc in NaCl and in NaOH solutions. Part I: corrosion layer characterization, Corrosion Sci. 52 (2010) 3984–3992.
[47] A.J. Drelich, P.K. Bowen, L. LaLonde, J. Goldman, J. Drelich, Importance of oxide film in endovascular biodegradable zinc stents, Surf. Innovat. 4 (2016) 133–140.